Prabhat KUMAR [1]

Modelling, analysis, and identification in a cracked and unbalanced Jeffcott rotor supported on foil bearings

This paper investigates on developing a novel model-based identification technique for the simultaneous identification of severe faults such as the unbalance in the rotor and transverse crack in the shaft supported on foil bearings. With plenty of advantages over rolling element bearings or fluid film bearings, foil bearings have been used as the supported bearings in rotating machines such as fuel cell-electric air compressors, blowers, expanders, air cycle machines, etc. In the present article, a rotor model consisting of a cracked and unbalanced rotor with a disc in the middle supported by foil bearings has been considered for easier understanding of online identification of faults in high-speed rotating machines. Dynamic equations of motion of the rotor-foil bearing system have been derived based on the equivalent stiffness concept of shaft-foil bearing, inertia force, unbalance force, and crack force relying on the switching crack concept. The solutions of the equations, i.e., time domain displacement responses, orbit plots, etc. have been obtained numerically using the Simulink inbuilt Runge-Kutta method for different values of spin speed of the rotor and ramp-up speeds. The shaft centreline orbit is found to have eight shaped and asymmetric about the axes due to presence of crack and unbalance faults. The force due to unbalance fault gets dominated over the crack force at the higher speeds. Moreover, the orbit line is also observed to be thicker at higher level of noise addition in the responses. As the switching crack force contains multiple harmonics, a full spectrum analysis has been done to investigate both the forward and backward rotor whirls. The frequency-based rotor displacement is utilized to illustrate an identification algorithm for the estimation of the dynamic coefficients of foil bearings, additive crack stiffness, and magnitude as well as phase of disc unbalance. The identification algorithm is found to be quite suitable for the estimation of system and faults parameters even with addition of different levels of noise signal and modelling errors.

✉ Prabhat KUMAR, e-mail: prabhat.kumar@nitmanipur.ac.in

[1] Department of Mechanical Engineering, National Institute of Technology Manipur, Imphal West, Manipur, India

1. Introduction

Various machines running at high speed are prone to different kinds of faults such as unbalance, transverse cracks, bearing and coupling misalignment, rub-impact, internal damping, mechanical looseness, etc. [1]. Bearings are the machine components that assist in supporting the rotating elements such as shafts associated with discs, flywheels, gears, and other revolving parts [2]. Since a long year back, traditional bearings have been employed to support the rotor. However, this paper uses air foil bearings, which is one of the current research trends [3–5]. Foil bearings work on the principle of hydrodynamic action of air, which consists of top foil, bump foil, and outer sleeve (refer Fig. 1). Relative motion between top foil and bump foil provides damping to the system and flexibility in bump foil during the rotor operation provides stiffness to the system [6]. As there is no requirement for lubricant in foil bearing, this becomes more effective and reliable in use in comparison to conventional bearings such as rolling contact bearings and fluid-film bearings. Foil bearing helps in rotating the rotor at ultra-high speeds and higher temperature zones [7]. There are fewer chances of wear and tear in the rotor-foil bearing system and also has a low maintenance cost. In modern days, foil bearings are commonly utilized in micro-turbines, air circulators, fuel cell blowers, and aerospace industries in the air cycle machine [8, 9].
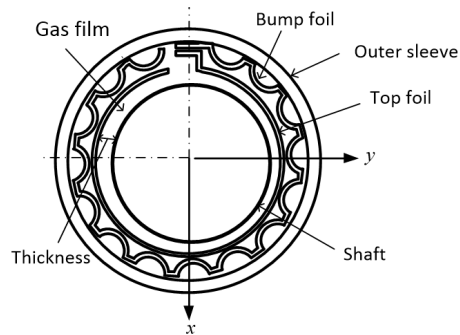

Fig. 1. Cross-sectional view of gas foil bearing

Peng and Carpino [10] utilized a perturbation method for obtaining linearized dynamic coefficient equations and calculating the stiffness and damping coefficients of gas-lubricated foil bearings. It was found that the elastic foundation could significantly reduce both the stiffness as well as damping constants of bearings. Rubio and Andres [11] performed experiments to determine the structural stiffness of bump-type foil bearings. It was observed that the single bump stiffness is the most sensitive to the dry friction coefficient as well as the bump length. Arora et al. [12] identified experimentally the dynamic coefficients of axial-type foil bearings. From the experimental results, one of the observations was made that the stiffness value was extremely high at the rotor's static position and the value

decreased with an increase in the shaft rotational speed. Later, an experimental work was executed by Balducchi et al. [13] in a rotor system supported by two foil bearings. They analysed unbalance responses with consideration of only in-phase imbalance masses, as there was a rapid heating issue considering the opposite-phase imbalance masses. Larsen et al. [14] proposed two different schemes for stability analysis of a rigid rotor mounted on foil bearings. The schemes include nonlinear time domain simulation as the first one and the frequency domain method as the second scheme. They have also shown that the bump structure compliance had a very strong influence on the journal lateral stability. In order to accurately design a foil bearing, the effect of air temperature was studied by Maraiy et al. [15] for describing the bearing performance. It was noticed that an increase in gas temperature leads to an increase in gas viscosity, which affects the foil-bearing performance. The performance was checked based on various parameters such as eccentricity ratio, length-to-diameter ratio, compliance coefficient, and bearing number. They have also explored the effect of increasing the number of bumps on bearing load carrying capacity. Further, Guo et al. [16] investigated the effects of the nominal radial clearance and foil structure on the rotor dynamic performance of a rotor-gas foil bearing system. Three test gas foil bearings with different radial clearance (30, 40, and 65 μm) were taken for testing. They observed that the values of dynamic coefficients increased with a decrease in the nominal clearance. Further, the measurements and predictions acquired by them indicated that the radial clearance and foil structure significantly affect the rotor dynamic performance of the rotor-foil bearing system. Li et al. [17] evaluated the static as well as the dynamic behaviour of gas foil bearings under the influence of a misalignment fault. It was noticed that when there is a large misalignment between the rotor and foil bearing, the gas film thickness and distribution in the pressure get immensely distorted. Martowicz et al. [18] utilized smart materials in gas foil bearings to enhance their capability and performance in terms of their mechanical as well as thermal characteristics. The working operation of gas foil bearings remained stable even for demanding excitations and environmental conditions. In the same year 2021, Kumar et al. [19] presented a sensitivity analysis and provided an optimum range of four design parameters (i.e., minimum film thickness, the ratio of angular extent at wedging, the angular extent of thrust pad, and rotational speed) of a gas foil thrust bearing for which it can have a maximum load-carrying capacity and low power loss using artificial intelligence techniques. They observed that these parameters have a significant effect on load-carrying capacity, power loss, and side leakage. Khamari et al. [20] presented a brief review on mathematical modelling and stability analysis of a rotor system supported by gas foil bearing. They have also described several analytical models used for simulating the performance of gas foil bearing as well as their correlations with experimental data. Afterward, Xu et al. [21] studied vibration characteristics control of hybrid radial gas foil bearing-rotor systems through both numerical and experimental works. It was concluded that the hybrid type bearing can minimize the shaft system vibration and enhance shaft sys-

tem stability. Recently, Guan et al. [22] performed rotordynamic analysis of a rotor supported by active bump-type foil bearings in the radial direction and bump-type thrust foil bearings in the axial direction. The effects of various disk misalignments on the minimum gas film thickness of the bump-type thrust foil bearings were also elaborated by them. Zhao et al. [23] developed a nonlinear model by considering frictional contacts inside the foil structure. This was done to explore the dissipation mechanism and dynamic characteristics of the rotor-gas foil bearing system. The model has taken into account the transient hydrodynamic pressure, rotor motion, and deflection of the foil structure. At last, they concluded that a large nominal clearance can help in eliminating the large amplitude subsynchronous vibrations. This can further ensure a more stable and reliable operation.

Crack is an important fault in the rotor. It may occur at a position where high stresses are present in the rotor and also occurs due to the fatigue of the shaft material during the excessive cycle of operations in the machine's life [24]. Timely detection and identification of cracks in the rotor plays a vital role in preventing expensive and catastrophic failure in the rotating machine, which helps in the proper working of industrial plants. Gasch [25] presented stability behaviour of a simple rotor having a disk in the middle with a transverse crack and forced vibrations due to the imbalance and to the crack based on the hinge model with no damping. Modelling of transverse crack is done with the switching crack concept, in which the crack gets opened and closed periodically in time. Paper [26] elaborated on the vibrational behaviour of a rotor system with a crack and active magnetic bearing (AMB) support mechanism. The peak value of response was obtained at twice as well as thrice the speed. Sekhar [27] proposed a model-based method for the identification of two cracks in the rotor system. The arrogant nature of the estimated equivalent forces at the two locations on the shaft was used to identify two cracks in the system. The identification method was used with the estimation of equivalent loads to identify the two cracks since the fast Fourier transform of the estimated equivalent force did not identify them together. Later, the same method was utilized by Pennacchi et al. [28] for the identification of transverse cracks present in industrial machines. They validated the identified results with experimental results obtained on a large test rig specially designed for dynamic behaviour analysis of the horizontal cracked rotor. Three different types of cracks were considered, i.e., crack having a slot of 34% depth, a partially breathing crack having a depth of 14% of the diameter, and a deep crack having a depth of 47% of the diameter. The proposed method was found to be effective, robust, and reliable with good accuracy for identifying the position and location of different cracks. Moreover, they also noticed that this method is suitable for large industry field applications, as only measurements in the bearings, or close to the bearings were required for this identification procedure. Researchers have also used the switching crack theory in structural dynamics. Further, the model-based estimation methodology was also used by researchers [29] for the purpose of crack and unbalance identification in an AMB-controlled rotating model. Peng and He [30] investigated the effect of positioning of breathing crack on the dynamic nature

of a cracked rotor in the presence of rotational damping. They have also examined the effects of the crack position on both the stiffness and the whirl motion of the breathing cracked rotor as well as on the rotor stability. A new technique based on squared gain of vibration amplitude was utilized by Gradzki et al. [31] to detect crack fault. They have performed both the experimental and numerical simulation to evaluate effectiveness of the proposed method. For removing environmental signals, i.e., sensor noise, external disturbances, etc. from the diagnostic model, the two time intervals were analysed. One was related to the operational signal and another was for environmental signal. However, they used a short time interval concept so that the environmental signal remains unchanged in those time intervals. The method was capable of detecting the crack fault in the existence of variable amplitude data and reasonably high measurement disruptions. It was also planned to perform experiments in the future and detect other faults such as misalignment and rub using this method. Thereafter, fifteen tree classification-based machine-learning algorithms were used for the localization and identification of crack on wind turbine blades [32]. The algorithms have taken the blade's vibration response as an input received from the piezoelectric accelerometer. They compared the obtained results with statistical, histogram as well as autoregressive moving average analysis. It was observed that the machine learning approach was very helpful and effective in the health monitoring of the wind turbine blade. This would enhance the harvest of wind power capacity and minimize downtime of the windmill. In the field of identification of crack fault in a gear system, researchers [33] detected a crack in a spur gear tooth by developing a three-degrees-of-freedom gear pair model. For model development purposes, they considered tooth backlash as well as nonlinearity in the bearing clearance. Later, Yang et al. [34] presented the vibrational dynamics of a transverse cracked hollow-shaft system by considering the parametric uncertainties. The rotor system consisted of one hollow shaft linked with two offset discs supported by conventional bearings. The finite element method was used to develop the dynamical equations of the rotor system. They have utilized the Polynomial Chaos Expansion technique to elucidate the uncertainties of the physical parameters in the rotor system. Further, the Harmonic Balance method was used for solving the system's equations of motion. It was observed that the uncertain parameters for the dynamical response were seriously affected by an increase in the crack depth. Zhang et al. [35] proposed a novel energy identification method to investigate a rotor system having a shallow-type transverse crack and flexible supports. They have applied the vibration energy method and a novel 3D energy model to examine the vibration characteristics of the cracked system, under the effect of rotating speed, crack depth, and crack location. Experimental works were also performed by them to validate the proposed theoretical methods. Recently, a model was developed by Qiao et al. [36] to identify the crack in a gear drive system in a wind turbine. It was remarked that the crack had a high impact on the mesh stiffness of the single-tooth contact zone. Han et al. [37] explored the breathing behaviour of a cracked rotor system under the influence of unbalance

disturbance. The unbalanced cracked rotor was found to have a 2×superharmonic resonance in the subcritical speed region, while the 3×superharmonic frequency component was observed to be weaker in the amplitude.

Unbalance fault is also one of the most critical faults in rotating machines, as the force due to this fault increases highly in amount with a slight increment in the speed. This force is equal to the product of mass, rotor eccentricity, and square of spin speed [38]. The system response also gets enhanced with increments in the unbalanced force. Hence, several researchers have investigated the dynamics analysis of the faulty system and different condition monitoring techniques for the identification of fault [39]. More than 80 years ago, Baker [40] proposed a mathematical model for determining unbalance corrections in machines, where the locations were difficult to identify through balancing machines. He applied this method to find unbalance corrections in an internal combustion engine crankshaft. Gupta et al. [41] developed a dual rotor test rig setup and determined experimentally the unbalance response, critical speeds and mode shape of the system. Experimental results were also compared with theoretical results and found to be reliable and effective. However, they did not consider the gyroscopic couple effects and rotary inertia. Thereafter, Shih and Lee [42] first measured the vibration signals of the pedestal and determined the discrete imbalance state of the rotating machine. However, the method was not found to be sensitive in the identification with noise corrupted signals. Zhou and Shi [43] reviewed different theoretical models for the rigid and flexible rotor balancing. They have claimed that the active balancing techniques can be used for controlling the vibration-induced rotor displacements. Later, an active control technique was employed by the researcher [44] to identify unbalance state in a Jeffcott rotor system. De Castro et al. [45] proposed a metaheuristic search algorithm for estimation of the unbalance magnitude and phase and its location in the shaft supported on hydrodynamic bearings. The method was observed to be robust in identifying the unbalance parameters and position along the rotor axis. Researchers [46] applied inverse problem for solving the estimation equation and finding the characteristics of rotor-bearing system's unbalance. They have also used Tikhonov regularization method to acquire stable results. Afterward, the unbalance in the rotor and misalignment in active magnetic bearing were identified in the published paper [47] by developing a novel trial misalignment approach. This approach was similar to the trial unbalance technique used for balancing. In recent years, Zhang et al. [48] presented a method based on signal purification for solving the dynamic balancing problem of a rotor. The signal purification technique included signal resampling and spectrum correction. They have also used this technique for suppressing vibration due to unbalance fault. Experiments were also performed on a test rig setup consisting of a rotor system linked with two discs and data acquisition as well as a processing device. Shun and Lei [49] also proposed an unsupervised deep Lagrangian network method for balancing the rotor. To introduce the prior knowledge of physical test rig setup, a Lagrangian layer was applied to the network. Both experimental and numerical works were

executed to validate the developed balancing method. Numerical simulation was done by considering a rotor system having four rigid discs and two ball bearings support. They used Newton's second law to establish equations of motion of the system. The responses like displacement, velocity, and acceleration were generated by solving equations of motion using the Runge-Kutta method. Output results of the rotor balancing through simulation and experiment proved that the technique was reasonable, costless, and user-convenient. Lin et al. [50] utilized a deep learning method for the identification of unbalance force in a hypergravity centrifuge structure. They have also developed a feature fusion framework and combined it with time domain signals for exploring the identification effect. It was found that the proposed approach is simple and quite reliable as compared to the conventional unbalanced force identification technique. This approach surpasses the concept of trial mass and model complexity. Similarly, Baltazar-Tadeo et al. [51] proposed an integrated rotor balancing method for the identification of unbalance force in a multi-degrees-of-freedom unbalanced and asymmetric rotor-bearing system. This method included the methodology of parameter algebraic identification and the traditional modal balancing approach. The developed algebraic identifier needed the displacement response as input data, in place of the vibration response obtained by putting trial weights in the traditional rotor balancing methods. Recently, Kang et al. [52] applied a dual augmented Kalman filter technique for simultaneous estimation of residual unbalance and bearing dynamic coefficients for a double-disk rotor-bearing system. The proposed method exhibited robust estimation capabilities, particularly when the system was operated under steady-state conditions. The percentage errors in the estimation of identifiable parameters were low and in the acceptable range.

By going through various published literature, it has been remarked that the papers are quite available in the field of stability analysis of foil bearings, the effect of gas temperature, number of bumps, eccentricity ratio, and misalignment in foil bearings. Research papers are also available in the identification of unbalance and crack faults in the supported conventional bearings as well as active magnetic bearings. Different techniques such as model-based methods, artificial intelligence techniques such as deep learning algorithms, machine learning algorithms, Kalman filter technique, and harmonic balance method, etc., were found to be used by researchers for solving dynamic equations of motion and severe fault identification. However, there is no publication found in the area of mathematical modelling and simultaneous identification of the rotor unbalance and crack in the rotor system with foil bearings support. Therefore, the novelty of the present work would be simultaneously identifying severe faults such as unbalance and crack malfunctions, as well as the supported bearing parameters in a rotor-foil bearing system, by estimating the unbalance magnitude and phase, crack additive stiffness, and stiffness and damping coefficients of foil bearings.

Hence, the present work discusses modelling, dynamic analysis, and identification in a cracked and unbalanced Jeffcott rotor system with a disc at the middle

supported by two foil bearings. Incorporating the equivalent stiffness concept of shaft and foil bearings and considering the forces due to inertia, unbalance, and crack faults, the dynamic equations of motion of the rotor-foil bearing system have been derived using Newton's law of motion. The mechanism of a switching crack has been utilized to analyse the effect of a transverse crack fault, which manifests multiple harmonics in the vibrational nature of the system. The displacement responses in the transverse directions (time domain spectrum and orbit plots) have been obtained using the Simulink^{TM} block diagram for different speeds and ramp-up speeds. Full spectrum data analysis has also been performed to transform the time domain response into the frequency domain, which gives rise to both the forward and backward rotor whirls. The main objective of the paper is to investigate the dynamic effects of unbalance and crack faults as well as to develop a model-based technique to identify them in a rotor system with foil bearing supports.

2. Rotor system modelling configuration

To develop a mathematical model for the exploration of an identification technique that can be used for the identification of various faults in high-speed rotating machinery, a rotor-foil bearing system has been considered. The rotor-model (as shown in Fig. 2) has been taken as a simple model to explore the dynamic vibrational analysis of an unbalanced and cracked single-disc Jeffcott rotor-foil bearing system and to illustrate the proposed identification methodology. Moreover, a faulty rotor system has been considered which can provide various information on time domain response signals, frequency spectrum, and orbit plots under the effect of unbalance and crack faults with foil bearing supports. This information may be helpful in understanding the dynamics of faulty gas turbines, air cycle machines in aircraft, etc., associated with the combined unbalance and crack faults. The considered rotor system consists of a shaft with a rigid disc at mid-span supported by two foil bearings (FBs) as depicted in Fig.2, where z represent the operating axis of rotor. The x- and y-directions represent for the vertical and horizontal directions, respectively. The shaft is assumed to be massless as compared to rigid disc mass. The rotor is having two transverse displacements along x and y directions. A transverse crack on the shaft is modelled as switching crack. Both foil bearings are considered to be identical. The stiffness and damping coefficients of foil bearings are also assumed to be speed-independent for brevity. In Fig. 2, the springs are shown at the locations of the foil bearings to represent their stiffness value k_b. The symbol k_0 represents the intact shaft stiffness. It can be observed from Fig. 2 that both foil bearings and shaft are in series combination. Hence, the equivalent stiffness of the rotor system, as experienced by disc, can be written as

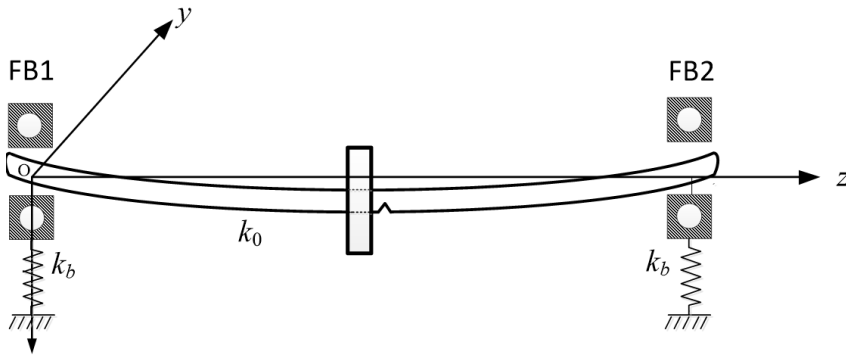$$k_{\text{eq}} = \frac{2k_0 k_b}{2k_b + k_0}.$$
(1)

Fig. 2. Schematic diagram of a cracked Jeffcott rotor system supported on foil bearings

Further, Fig. 3a shows the stationary and rotating coordinate systems for crack fault in the system. Fig. 3b shows a cross-sectional view of the rotor and disc with the relative position of unbalance and crack fault, where e is the eccentricity of the rotor and β is the angle between eccentricity line and crack centreline.
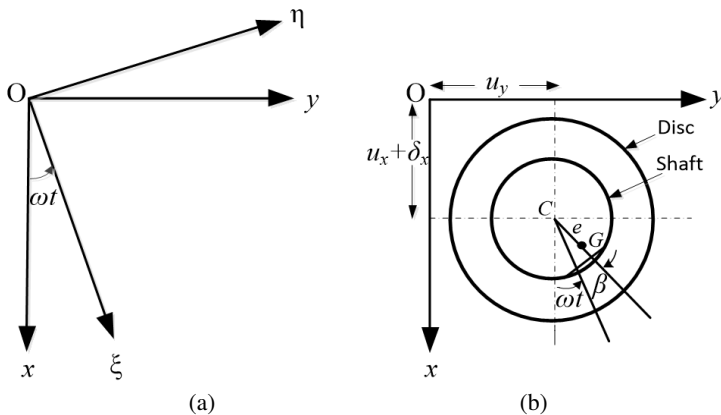

(a)   (b)

Fig. 3. (a) Stationary and rotating coordinate references; (b) Relative position of unbalance and crack

2.1. Crack model

In line with the derivation of the stiffness matrix of the cracked shaft, as done in Gasch [53] using transformation between rotating and inertial coordinate systems by referring to Fig. 3a, the matrix can be expressed as

$$\mathbf{K}(t) = \mathbf{K}_{\text{eq}} + \Delta\mathbf{K}_c(t) = \begin{bmatrix} k_{\text{eq}} & 0 \\ 0 & k_{\text{eq}} \end{bmatrix} - \frac{1}{2}s_c(t)\Delta k_{\xi} \begin{bmatrix} 1 + \cos(2\omega t) & \sin(2\omega t) \\ \sin(2\omega t) & 1 - \cos(2\omega t) \end{bmatrix}, \quad (2)$$

where, k_{eq} is the equivalent stiffness of shaft and foil bearings. Δk_{ξ} denotes loss in the shaft stiffness due to crack in the direction of crack front, ξ. $s_c(t)$ is steering

function for crack having value 0 and 1 for opening and closing of crack respectively. $\Delta \mathbf{K}_c(t)$ denotes shaft stiffness matrix due to crack only.

Displacement of the rotor centre, $\mathbf{q}(t)$, can be written using Fig. 3b as

$$\mathbf{q}(t) = \Delta \mathbf{q}(t) + \mathbf{q}_0 \tag{3}$$

with $\mathbf{q}(t) = \begin{Bmatrix} x(t) \\ y(t) \end{Bmatrix}$, $\Delta \mathbf{q}(t) = \begin{Bmatrix} u_x(t) \\ u_y(t) \end{Bmatrix}$, $\mathbf{q}_0 = \begin{Bmatrix} \delta_x \\ 0 \end{Bmatrix}$.

3. Equations of motion of the rotor-foil bearing system

Equations of motion of the rotor-foil bearing system in terms of static deflection (δ_x) and vibration induced displacements (u_x and u_y) can be written as

$$\mathbf{M}\ddot{\mathbf{q}}(t) + \mathbf{C}\dot{\mathbf{q}}(t) + \mathbf{K}(t)\mathbf{q}(t) = \mathbf{f}_{st} + \mathbf{f}_{unb}(t), \tag{4}$$

with

$$\mathbf{M} = \begin{bmatrix} m & 0 \\ 0 & m \end{bmatrix}, \quad \mathbf{C} = \begin{bmatrix} 2c_b & 0 \\ 0 & 2c_b \end{bmatrix}, \quad \mathbf{f}_{st} = \begin{Bmatrix} mg \\ 0 \end{Bmatrix}, \quad \mathbf{f}_{unb}(t) = me\omega^2 \begin{Bmatrix} \cos(\omega t + \beta) \\ \sin(\omega t + \beta) \end{Bmatrix}.$$

On substituting Eqs. (2) and (3) into Eq. (4) and then, neglecting smaller terms $\Delta \mathbf{K}(t)\Delta \mathbf{q}(t)$ (this term is neglected because, in a heavy rotor, the static deflection δ_x is large as compared to vibration-induced displacements, which is known as the weight dominance effect [53]) as well as equating $\mathbf{K}_{eq}\mathbf{q}_0 = \mathbf{f}_{st}$, we get

$$\mathbf{M}\Delta\ddot{\mathbf{q}}(t) + \mathbf{C}\Delta\dot{\mathbf{q}}(t) + \mathbf{K}_{eq}\Delta\mathbf{q}(t) = \mathbf{f}_{cr}(t) + \mathbf{f}_{unb}(t), \tag{5}$$

where the force due to crack fault is

$$\mathbf{f}_{cr}(t) = -\Delta\mathbf{K}_c(t)\mathbf{q}_0 = \frac{1}{2}\Delta k_\xi s_c(t)\delta_x \begin{Bmatrix} 1 + \cos 2\omega t \\ \sin 2\omega t \end{Bmatrix}. \tag{6}$$

3.1. Steering function for the transverse crack

A transverse crack is assumed as a switching crack [53]. The opening and closing of the switching crack are supposed to be modelled as hinge-type when the crack depth is assumed to be less than half of the shaft radius ($a/R < 0.5$) [25], where a is the crack depth and R is the radius of the shaft. Here, it is assumed that the crack toggles between full open and full crack positions, mimicking the opening and closing of a hinge based on the loading condition. A switching crack is approximated by a rectangular waveform (Gasch [53]) as shown in Fig. 4. The switching function ($s_c(t)$) can be expressed in the mathematical form as

$$s_c(t) = 0.5000 + 0.6366\cos(\omega t) - 0.2120\cos(3\omega t) + 0.1273\cos(5\omega t)$$
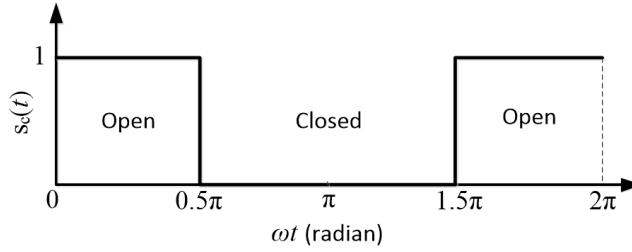$$- 0.0910\cos(7\omega t) + 0.0707\cos(9\omega t) - \ldots \tag{7}$$

Fig. 4. Variation of crack switching function, $s_c(t)$ with shaft rotation [53]

In complex form, the crack force, i.e., Eq. (6), can be expressed in a series of multiple harmonics,

$$f^c_{\text{crack}}(t) = \Delta k_\xi \delta_x \begin{pmatrix} \dots 0.009e^{-\text{j}5\omega t} - 0.021e^{-\text{j}3\omega t} + 0.106e^{-\text{j}\omega t} + 0.250 \\ + 0.319e^{\text{j}\omega t} + 0.250e^{\text{j}2\omega t} + 0.106e^{\text{j}3\omega t} \\ - 0.021e^{\text{j}5\omega t} + 0.009e^{\text{j}7\omega t} + \dots \end{pmatrix}. \quad (8)$$

In notational form

$$f^c_{\text{crack}} = \Delta k_\xi \delta_x \sum_{i=-n}^{i=+n} p_{ic} e^{\text{j}i\omega t},$$

where p_{ic} is the i-th harmonic coefficient of the crack excitation force.

3.2. Analysis of forced responses

Forced vibration analysis of the rotor system can be done using Eq. (5). For less computational effort, the displacements u_x and u_y can be written in complex form as

$$r(t) = u_x(t) + \text{j}u_y(t). \quad (9)$$

The complex form of Eq. (5) is written as

$$m\ddot{r} + 2c_b\dot{r} + k_{\text{eq}}r = f^c_{\text{cr}} + f^c_{\text{unb}} \quad (10)$$

with

$$f^c_{\text{unb}} = me\omega^2 e^{\text{j}(\omega t+\beta)},$$

where j denotes a complex number equal to $\sqrt{-1}$. The salient reason for expressing the equations of motion (5) in complex form is to explore the frequency based full spectrum analysis, which will be further utilized in the developed identification algorithm for the estimation purpose. It is briefly explained in the next section. Eq. (10) has been solved by building a SIMULINK$^{\text{TM}}$ model to generate the rotor displacement response of the system in the time domain. Response in the time domain can be used to obtain the harmonics of the crack excitation function. The response $R_i(t)$ for a particular harmonic of crack excitation force is assumed as

$R_i(\omega)e^{ji\omega t}$. Thus, at any instant of time, the relationship between the complex displacement signal and its individual complex harmonics are given as

$$r(t) = R_{-n}e^{-nj\omega t} + \cdots + R_{-5}e^{-5j\omega t} + R_{-3}e^{-3j\omega t} + R_{-1}e^{-1j\omega t} + R_0e^{-0j\omega t}$$
$$+ R_1e^{1j\omega t} + R_2e^{2j\omega t} + R_3e^{3j\omega t} + R_5e^{5j\omega t} + \cdots + R_ne^{nj\omega t}. \tag{11}$$

Assuming

$$R_i(t) = R_i(\omega)e^{ji\omega t}; \ \dot{R}_i(t) = ji\omega R_i(\omega)e^{ji\omega t}; \ \ddot{R}_i(t) = -i^2\omega^2 R_i(\omega)e^{ji\omega t}. \tag{12}$$

4. Model based identification algorithm of the considered rotor-foil bearing system

Inverse engineering problem is nothing but transforming a mathematical form of the equations of motion of the system into a regression form. The system parameters such as the damping coefficient of bearing (c_b), equivalent stiffness of the system (k_{eq}), additive crack stiffness (Δk_ξ), and unbalance (phase and magnitude, i.e., e, β) can also be simultaneously identified utilizing grey box identification method [54]. Estimation of foil bearing stiffness coefficient (k_b) can also be done using rearrangement of equation (1) as

$$k_b = \frac{k_{eq}k_0}{2(k_0 - k_{eq})}, \tag{13}$$

where k_0 is the stiffness value of the intact shaft, which is the known parameter.

4.1. Estimation of rotor displacement harmonics from full spectrum

FFT technique of MATLAB^{TM} has been utilized to convert the time-domain displacement responses into frequency-domain responses [55]. Further, the full spectrum analysis from FFT is required, because Eq. (11) shows that the displacement signals have both positive and negative harmonic frequencies. A complex number is the output of FFT analysis, which includes magnitude and phase. Due to the linearity nature of FFT, the magnitude of the response remains the same but the phase changes during the transformation of the time domain analysis into frequency domain analysis. So, a reference signal is included with FFT analysed signal to get the correct phase of the response in the frequency domain.

4.2. Mathematical procedure for estimation of system parameters

The complex form of the rotor displacement in the frequency domain captured from the full spectrum as well as the complex form of unbalance force are separated into the real and imaginary parts as

$$R_i = R_{i,\text{Re}} + jR_{i,\text{Im}},$$
$$me\omega^2 e^{j\beta} = m\omega^2(e\cos\beta + je\sin\beta) = m\omega^2(e_{\text{Re}} + je_{\text{Im}}). \tag{14}$$

Substituting Eqs. (12) and (14) into Eq. (10) we get fot ($i \neq 1$) and ($i = 1$) as

$$
\begin{aligned}
(R_{i,\text{Re}} + jR_{i,\text{Im}})\left[(-i^2\omega^2 m) + (j(ji2\omega c_b) + (k_{\text{eq}})\right] &= \Delta k_\xi \delta_x p_{ic}, \\
(R_{i,\text{Re}} + jR_{i,\text{Im}})\left[(-\omega^2 m) + (j(j2\omega c_b) + (k_{\text{eq}})\right] &= \Delta k_\xi \delta_x p_{ic} + m\omega^2(e_{\text{Re}} + je_{\text{Im}})
\end{aligned}
\tag{15}
$$

Now, rearranging both equations of Eq. (15) in such a way that the known parameters (m) related terms are on the right-hand side and all the terms accompanied with the identifiable parameters that have to be estimated (i.e., c_b, Δk_ξ, e_{Re}, e_{Im}, k_{eq}) are on the left-hand side of the equations. Further, separating them into real and imaginary parts for 'p' number of harmonics, and next rewriting all equations in the matrix form to perform the linear regression analysis as

$$
\mathbf{A}_{(p \times q)} \mathbf{x}_{(q \times 1)} = \mathbf{b}_{(p \times 1)},
\tag{16}
$$

where, q is the number of unknowns. It is noticeable that the number of unknowns is less than the number of equations, so it is a class of overdetermined ($p > q$) system of equations. Thus, Eq. (16) can be solved to determine the identifiable parameters using the least-squares fitting technique as

$$
\mathbf{x} = \left(\mathbf{A}^T \mathbf{A}\right)^{-1} \mathbf{A}^T \mathbf{b},
\tag{17}
$$

$$
\mathbf{A} = \begin{bmatrix}
-2\omega R_{1,\text{Im}} & -\delta_x p_{1c} & -m\omega^2 & 0 & R_{1,\text{Re}} \\
0 & -\delta_x p_{0c} & 0 & 0 & R_{0,\text{Re}} \\
-4\omega R_{2,\text{Im}} & -\delta_x p_{2c} & 0 & 0 & R_{2,\text{Re}} \\
-6\omega R_{3,\text{Im}} & -\delta_x p_{3c} & 0 & 0 & R_{3,\text{Re}} \\
-10\omega R_{5,\text{Im}} & -\delta_x p_{5c} & 0 & 0 & R_{5,\text{Re}} \\
\vdots & \vdots & \vdots & \vdots & \vdots \\
2\omega R_{-1,\text{Im}} & -\delta_x p_{-1c} & 0 & 0 & R_{-1,\text{Re}} \\
6\omega R_{-3,\text{Im}} & -\delta_x p_{-3c} & 0 & 0 & R_{-3,\text{Re}} \\
10\omega R_{-5,\text{Im}} & -\delta_x p_{-5c} & 0 & 0 & R_{-5,\text{Re}} \\
\vdots & \vdots & \vdots & \vdots & \vdots \\
2\omega R_{1,\text{Re}} & 0 & 0 & -m\omega^2 & R_{1,\text{Im}} \\
0 & 0 & 0 & 0 & R_{0,\text{Im}} \\
4\omega R_{2,\text{Re}} & 0 & 0 & 0 & R_{2,\text{Im}} \\
6\omega R_{3,\text{Re}} & 0 & 0 & 0 & R_{3,\text{Im}} \\
10\omega R_{5,\text{Re}} & 0 & 0 & 0 & R_{5,\text{Im}} \\
\vdots & \vdots & \vdots & \vdots & \vdots \\
-2\omega R_{-1,\text{Re}} & 0 & 0 & 0 & R_{-1,\text{Im}} \\
-6\omega R_{-3,\text{Re}} & 0 & 0 & 0 & R_{-3,\text{Im}} \\
-10\omega R_{-5,\text{Re}} & 0 & 0 & 0 & R_{-5,\text{Im}} \\
\vdots & \vdots & \vdots & \vdots & \vdots
\end{bmatrix}
; \mathbf{b} = \begin{Bmatrix}
\omega^2 m R_{1,\text{Re}} \\
0 \\
4\omega^2 m R_{2,\text{Re}} \\
9\omega^2 m R_{3,\text{Re}} \\
25\omega^2 m R_{5,\text{Re}} \\
\vdots \\
\omega^2 m R_{-1,\text{Re}} \\
9\omega^2 m R_{-3,\text{Re}} \\
25\omega^2 m R_{-5,\text{Re}} \\
\vdots \\
\omega^2 m R_{1,\text{Im}} \\
0 \\
4\omega^2 m R_{2,\text{Im}} \\
9\omega^2 m R_{3,\text{Im}} \\
25\omega^2 m R_{5,\text{Im}} \\
\vdots \\
\omega^2 m R_{-1,\text{Im}} \\
9\omega^2 m R_{-3,\text{Im}} \\
25\omega^2 m R_{-5,\text{Im}} \\
\vdots
\end{Bmatrix}
; \mathbf{x} = \begin{Bmatrix}
c_b \\
\Delta k_\xi \\
e_{\text{Re}} \\
e_{\text{Im}} \\
k_{\text{eq}}
\end{Bmatrix}
$$

After finding the value of k_{eq} (i.e., using Eq. (17)), the value of the stiffness coefficient of foil bearings can be obtained from Eq. (13). Thus, it is possible to determine the values of unbalance fault parameters, stiffness and damping coefficients of foil bearings as well as crack additive stiffness.

5. Generation of simulated responses and identification

Fig. 5 shows a developed SIMULINK^{TM} model to generate the rotor displacement response in the time domain using Eq. (10). Blocks in the model perform various important functions. The clock is a source block, which outputs the present simulation time. The gain triangular block is utilized for multiplication purposes. The spin speed ω has been multiplied by the clock to give ωt as output, which is the further common input to the subsystems such as unbalance force and crack force for exploring the dynamics of the defined rotor system. Summation and subtraction of forces based on the derived equations of motion have been performed utilizing the add block. The inverse of the mass parameter is multiplied with the add block to acquire the acceleration response of the rotor-foil bearing system. Further, one integrator block is used to obtain the velocity responses, and then again another integrator block is utilized for obtaining the displacement responses of the system in x and y directions. The correct phase in full spectrum analysed responses has been obtained with the help of a multi-harmonic reference signal generator, which is also included in the model. The workspace blocks save the real or complex data of responses. Overall, this model is quite effective and advantageous.
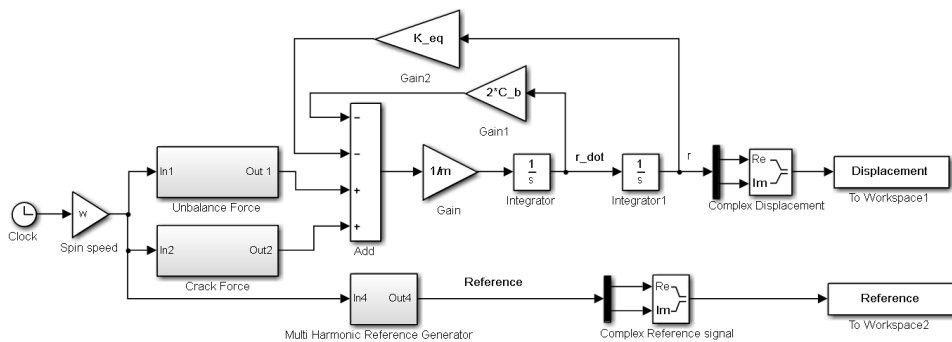

Fig. 5. Simulink model of the rotor-foil bearing system

5.1. Numerical results analysis of the cracked rotor-foil bearing system

This section describes briefly the numerically generated responses for the considered system presented in Fig. 2. The time domain displacements of the rotor system in x and y directions have been determined using a fourth-order Runge-Kutta

ordinary differential equation solver with a fixed step size of 0.0001 s following Table 1 numerical data.

Table 1. Rotor-foil bearing system data for the numerical simulation

System parameters	Assumed values	System parameters	Assumed values
Density of shaft and disc material (mild steel), ρ	7850 kg/m^3	Elastic modulus of shafts and disc material (mild steel), E	2.1×10^{11} N/m^2
Shaft diameter, d	17.7 mm	Shaft length, l	400 mm
Disc diameter, D	115.2 mm	Disc thickness, t	15 mm
Rotor mass (shaft and disc), m	2 kg	Stiffness coefficient of foil bearing, k_b	1×10^6 N/m
Disc eccentricity, e	10×10^{-6} m	Damping coefficien t of foil bearing, c_b	120 N s/m
Shaft static deflection, δ_x	3.567×10^{-5} m	Stiffness of intact shaft, k_0	7.59×10^5 N/m
Unbalance phase, β	30° deg.	Additive crack stiffness, δk_ξ	1.518×10^5 N/m

Rotor dimensions and their physical properties are based on the laboratory rotor test kit developed by the researchers [56]. The mass of rotor (shaft and disc) is calculated from the values of material density, diameter, length, and thickness properties. The value of shaft intact stiffness is calculated with the values of the moment of inertia of the round shaft, modulus of elasticity, and length of the shaft. The value of shaft static deflection (i.e., 3.567×10^{-5} m) is obtained by dividing the weight of the rotor (mg) by the equivalent stiffness of the shaft-foil bearing system (k_{eq}). For the numerical simulation in this paper, the additive crack stiffness (Δk_ξ) is taken as 20% of the original stiffness of the shaft (k_0). It is found from various published papers that researchers have also considered the value of additive crack stiffness in the range of 25% to 40% of the intact stiffness of the shaft (refer to [54, 57, 58]). A lower percentage of additive crack stiffness relative to the original shaft stiffness demonstrates the lower value of crack depth. However, Gasch [53] discussed that the exact value of crack additive stiffness can be determined experimentally by measuring the natural frequencies of the rotor system with open and closed cracks, using the following equation:

$$\left(\frac{\omega_\xi}{\omega_0}\right)^2 = 1 - \frac{\Delta k_\xi}{k_0}, \tag{18}$$

where ω_ξ and ω_0 represent the natural frequency of the rotor system in the presence of an open crack and a completely closed crack or a healthy rotor system without crack, respectively. As the present paper is a demonstration of theoretical and numerical works, therefore, the additive crack stiffness is assumed to be 20% of the intact shaft stiffness. Apart from this, the values of foil bearing's stiffness and

damping coefficients are taken from the paper [10]. The displacement responses of the rotor system in the x and y directions together with their respective orbit plots at a shaft spin speed of 280 rad/s are represented in Fig. 6.
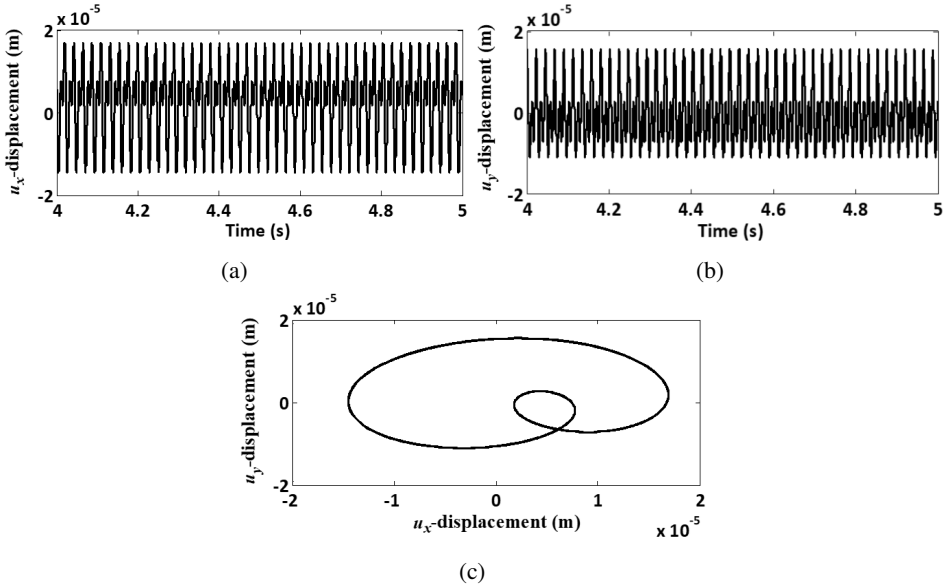

Fig. 6. Generated numerical responses at a spin speed of 280 rad/s: (a) x-direction time domain displacement; (b) y-direction time domain displacement (c) Shaft centreline orbit

The responses of the rotor along two orthogonal directions and the orbit plots for shaft centre displacement play a vital role in predicting and detecting the rotor's working condition. The maximum value of displacement response in the x-direction is 1.69×10^{-5} m and the highest value of displacement in the y-direction is 1.55×10^{-5} m. As it can also be remarked from Fig. 6c, the shaft centreline orbit is eight-shaped and simultaneously asymmetric about axes, so these orbit plots are helpful to indicate the crack fault in the rotor. A similar kind of eight-shaped orbit and the time domain displacement spectrum can also be seen in the paper [59]. This shows the accuracy of the results in the presence of a crack fault. Further, to explore the effect of the crack in the unbalanced rotor, the simulation has been also run for the case of without crack and with crack by putting the values of Δk_{ξ} as zero and non-zero in Eq. (6). The orbital response by considering only unbalance fault and unbalance as well as crack faults together is shown in Fig. 7. The highest value of vertical direction displacement without crack condition is only 3.93×10^{-6} m, whilst the maximum displacement value with crack is 1.69×10^{-5} m. Therefore, the percentage increase in the response is 76.75%., which is a considerable value. Therefore, it becomes very much desirable for a researcher to detect crack fault in a rotor-foil bearing system. Moreover, the orbit shape of only unbalance response looks circular in shape. It is obvious due to the similar harmonic nature of equations
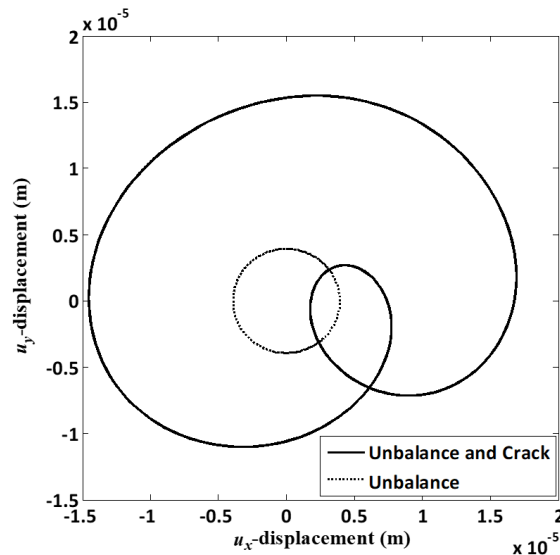
Fig. 7. Orbital response exhibiting the effect of crack fault
in the unbalanced rotor at a spin speed of 280 rad/s

of motion in the vertical and horizontal directions. The circular type displacement orbit is also observed in the article [58] for considering only unbalance fault in a Jeffcott rotor-conventional bearings system with an offset disc and AMB at the disc location. In this paper, the foil bearings were also assumed to be isotropic and similar in nature while development of the mathematical model of the system.

Further, the four different speeds of the rotor are also chosen in the simulation work to study the cracked and unbalanced rotor vibrational behaviour. The values of the speed taken are 150 rad/s, 200 rad/s, 280 rad/s and 370 rad/s. The displacement orbits at these speeds captured from the simulation work is presented in Fig. 8. It can be noticed from Fig. 8 that the crack fault is showing overpowering nature over the unbalance fault at the lower speeds (i.e., Fig. 8a, 8b and 8c). However, the force due to unbalance fault gets dominated over the force due to crack fault at the higher speed. That's why the shape of orbital response at the spin speed of 370 rad/s is observed to be elliptical in Fig. 8d. Apart from running the numerical simulation at a single speed one by one and analysing the responses from Fig. 6, Fig. 7 and Fig. 8, the rotor is also accelerated with an angular acceleration of 12.50 rad/s^2 and an initial spin speed of 5 rad/s. Thus, the ramp-up speed of the rotor varies from 5 rad/s to 380 rad/s. The time domain vertical (x) and horizontal (y) displacement responses and orbit plot at the disc location for the ramp-up speed are represented in Fig. 9 and Fig. 10, respectively. A similar kind of displacement response in the time domain for the ramp-up speed can be observed in the published literature [60].

Furthermore, to mimic the response that can be received from the actual test rig setup, the different percentages of white Gaussian noise (i.e., 3%, 5%, and 10%)
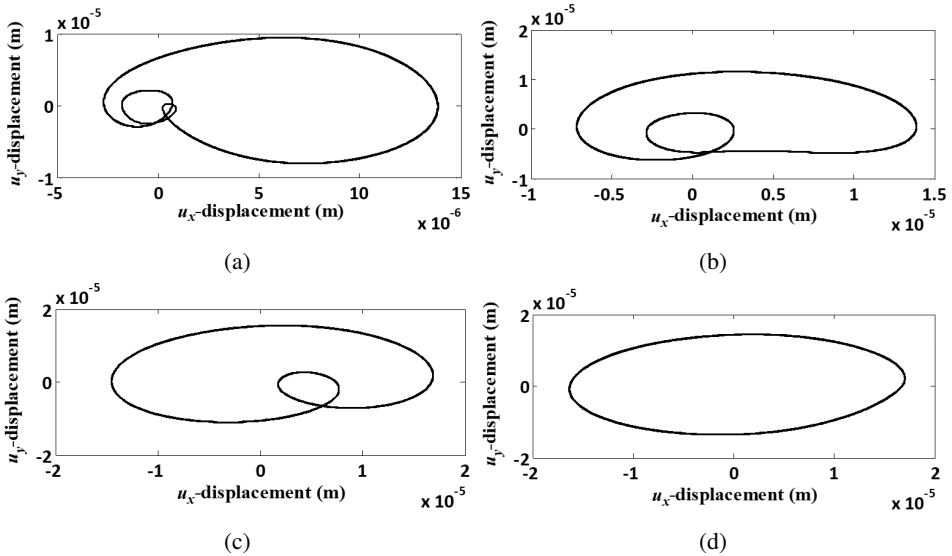
Fig. 8. Displacement orbit plots at the rotor spin speed of: (a) 150 rad/s, (b) 200 rad/s, (c) 280 rad/s, (d) 370 rad/s
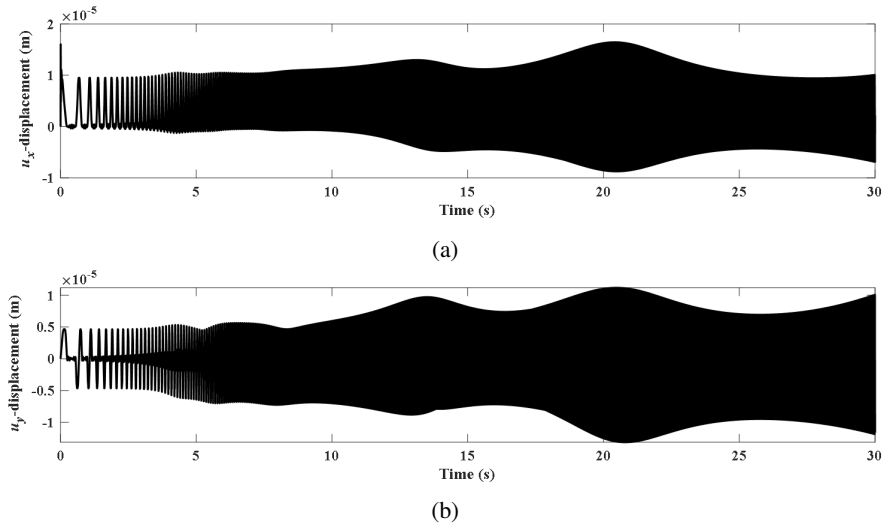

Fig. 9. Displacement response in the time domain for the ramp-up speed from 5 rad/s to 380 rad/s: (a) x-direction (b) y-direction

have been added to the time domain displacement signals. The concept of adding Gaussian noise in the numerical simulation is given as follows [36] (for example, an addition of 3% noise):

$$B_i = A_i + 0.01 \times A_i \times R_i; \quad -1.5 \leqslant R_i \leqslant 1.5, \tag{19}$$
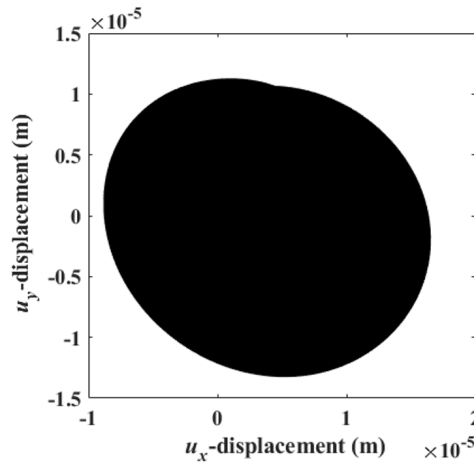
Fig. 10. Orbital response for the ramp-up speed from 5 rad/s
to 380 rad/s

where A_i and B_i, respectively, represent the clean displacement signal (without noise) and the displacement signal in which 3 percent (3%) random noise is added. The Gaussian random noise signal R_i (with $i = 1, 2, \ldots, n$) is generated from the normal distribution concept based on the size of A_i. Similarly, the random noise 5% and 10% have been added to the displacement signal. The orbital responses with the addition of 3%, 5%, and 10% noise at the spin speed of 280 rad/s are given in Fig. 11. The orbit looks more thicker and having a maximum value of displacement response (2.1×10^{-5} m in the x-direction and 1.93×10^{-5} m in the y-direction) at the highest magnitude of noise addition (i.e., 10% noise). This statement can be validated by the results presented in the paper [61].
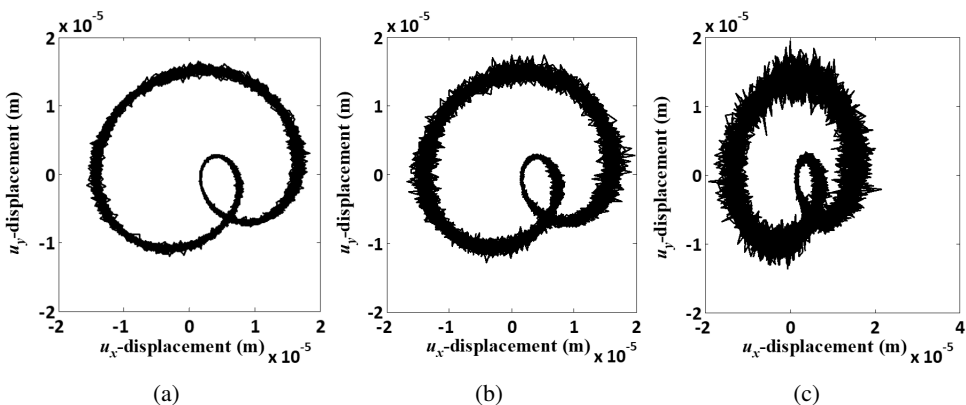
Fig. 11. Displacement orbits with the addition of different levels of noise at a spin speed of 280 rad/s: (a) 3% noise, (b) 5% noise, (c) 10% noise

5.2. Identification of crack, unbalance and foil bearing parameters

The simulation was run for 5 s using Table 1 parameters. The responses in the time domain for the duration from 4 s to 5 s (i.e., 1 s time length) were taken into consideration for further analysis. The time domain responses associated with Eq. (9) were converted to frequency domain assisted with the FFT function of MATLAB^{TM}. Further, the full spectrum analysis [62] has been performed to exhibit the responses at negative frequency harmonics together with positive frequency harmonics.

Full spectrum for the displacement signal with its amplitude and phase is shown in Fig. 12. The phase correction method explained by Singh and Tiwari [54] has been utilized to plot the phase diagrams for the displacement response of the system. The multiharmonic nature of the response in a full spectrum plot mainly depends on the steering function, i.e., Eq. (7) chosen for exploring the nature of the crack force. Table 2 summarizes the values of rotor displacement harmonics (R_i) with magnitudes and phases for several harmonics captured from full spectrum analysis. It can be observed from Fig. 12a that the magnitude of the displacement at twice of spin speed, i.e., at 560 rad/s is found to be maximum which represents the presence of the crack fault in the rotor system. The peak value of displacement is 8.45×10^{-6} m at a spin speed of 560 rad/s which can be noticed from Table 2. Further, the real and imaginary components of displacement response adopted from the magnitude and corrected phases for several harmonics of Table 2 have been utilized in the identification equation (16) for estimating the values of identifiable parameters at a single spin speed. The assumed and identified values of the system parameters derived from the developed algorithm with the percentage error for the clean signal are depicted in Table 3. It is observable that the identification of system parameters is robust and quite effective for a single spin speed, i.e., 280 rad/s. The
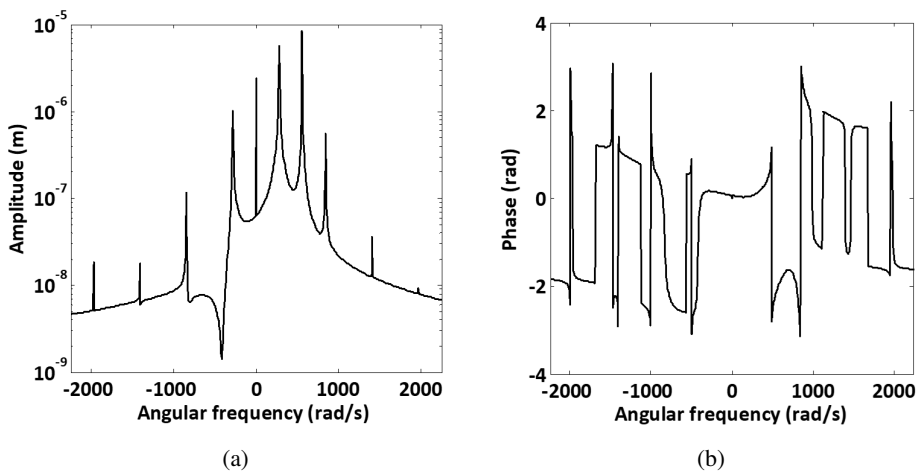

Fig. 12. Plots using full spectrum analysis: (a) displacement amplitude; (b) displacement phase

Table 2. Displacement harmonics obtained in the frequency domain

Harmonics (i)	Displacement (R_i)	
	Amplitude (m)	Phase (deg)
0	2.40×10^{-6}	−0.057
1	5.74×10^{-6}	4.70
2	8.45×10^{-6}	−120.21
3	5.61×10^{-7}	−169.11
5	3.62×10^{-8}	−1.33
7	9.20×10^{-9}	126.12
−1	1.01×10^{-6}	9.69
−3	1.17×10^{-7}	−9.97
−5	1.79×10^{-8}	−166.53

Table 3. Percentage error of identified values with respect to assumed values for clean signal

Parameters	Assumed values	Identified values for clean signal
Foil bearing damping coefficient, c_b	120 (Ns/m)	120.035
	% error	0.03%
Foil bearing stiffness coefficient, k_b	1×10^6 (N/m)	1×10^6
	% error	0.00%
Additive crack stiffness, Δk_ξ	1.518×10^5 (N/m)	1.5181×10^5
	% error	0.009%
Unbalance eccentricity, e	10×10^{-6} (m)	9.98×10^{-6}
	% error	−0.20%
Unbalance phase, β	30 (deg)	30.09
	% error	0.30%

estimation of foil bearing parameters, i.e., damping coefficient (c_b) and stiffness coefficient (k_b) is good. The percentage error for these parameters is 0.03% and 0% only, which is very much acceptable. It can be noticed that the additive crack stiffness (Δk_ξ) which is the indicator for the crack fault in the considered rotor system has also been estimated excellently. The percentage error concerning the identified value is only 0.009%. Moreover, the unbalance parameters (e, β) are also identified very accurately, with percentage errors of −0.2% and 0.3%, respectively.

To mimic the identification results from a real condition of test setup, three different noise levels, i.e., 3%, 5%, and 10% have been added to the displacement signals obtained from the simulation work. In a practical situation, the noise can come from the nearby environment, neighbouring machines in running condition, any kind of maintenance work, etc. The identified values of foil bearing stiffness

and damping constants, additive crack stiffness and unbalance parameters with the addition of noise signals are given in Table 4. The same table also presents the percentage deviation in the identified values relative to assumed ones. It has been found that the highest percentage deviation in the identified value of c_b is 1.992% only with the addition of 10% noise. The parameter k_b has been identified very accurately with percentage errors varying from -0.4% to -1.1% only with the addition of noise signals. The percentage deviation of the crack parameter varies from 0.916% to 3.03%. Besides this, the unbalance eccentricity and phase have been identified with the highest deviations of -8.77% and 8.90% at 10% noise addition. However, these values are quite acceptable and under limit. Finally, it can be also remarked that a higher percentage of noise signal addition gives more deviation in the identified values.

Table 4. Percentage error of identified values with respect to assumed values with noise signal

Parameters	Assumed values	Identified values for 3% noise	Identified values for 5% noise	Identified values for 10% noise
c_b	120 (Ns/m)	120.75	121.219	122.39
	% error	0.625%	1.016%	1.992%
k_b	1×10^6 (N/m)	0.996×10^6	0.994×10^6	0.989×10^6
	% error	-0.400%	-0.600%	-1.100%
Δk_ξ	1.518×10^5 (N/m)	1.5319×10^5	1.5411×10^5	1.564×10^5
	% error	0.916%	1.522%	3.030%
e	10×10^{-6} (m)	9.718×10^{-6}	9.547×10^{-6}	9.123×10^{-6}
	% error	-2.820%	-4.530%	-8.770%
β	30 (deg)	30.82	31.33	32.67
	% error	2.733%	4.433%	8.900%

Various operational constraints, measurement errors, and simplified assumptions in the model can also cause errors in the estimated values. Therefore, to overcome these issues, the three different levels of modelling or bias errors (i.e., 3%, 5%, and 10%) are also added to the system parameters such as density, modulus of elasticity, equivalent stiffness constant, etc. The identified values of faults and bearing parameters with the addition of bias errors are given in Table 5. It can be seen that all parameters have been identified precisely even with the addition of a high percentage of bias error. Even there was no error in the identification of the stiffness constant of the foil bearing. Various researchers [63–65] have used model-based identification methodology for the identification of unbalance, crack in rotor-conventional bearings support, AMB misalignment, and coupling misalignment faults. They have also identified the system and fault parameters with the addition of noise signals and modelling errors. Anyhow, they did not consider the concept of utilizing foil bearing to support the rotor. However, a similar kind

Table 5. Percentage error of identified values with respect to assumed values with the addition of modelling or bias error

Parameters	Assumed values	Identified values for 3% bias error	Identified values for 5% bias error	Identified values for 10% bias error
c_b	120 (Ns/m)	120.035	120.034	120.033
	% error	0.03%	0.028%	0.0275%
k_b	1×10^6 (N/m)	1×10^6	1×10^6	1×10^6
	% error	0.00%	0.00%	0.00%
Δk_ξ	1.518×10^5 (N/m)	1.5059×10^5	1.498×10^5	1.477×10^5
	% error	-0.800%	-1.318%	-2.700%
e	10×10^{-6} (m)	9.98×10^{-6}	9.98×10^{-6}	9.98×10^{-6}
	% error	-0.20%	-0.20%	-0.20%
β	30 (deg)	30.09	30.09	30.09
	% error	0.30%	0.30%	0.30%

of deviations in the estimated parameters were also observed by them in different kinds of faults. This shows the relevancy of the results presented in this paper. Therefore, the proposed estimation algorithm is one of the most salient and powerful techniques in identifying the unbalance and crack faults as well as stiffness and damping coefficients of foil bearings in a rotor system.

6. Conclusions

To overcome several operational constraints of traditional bearings, such as the low reliability and high maintenance of machines, friction losses due to lubrication, and wear and tear of bearing materials, this paper proposed the foil bearing technology to support a rotor system. In this direction, mathematical modelling and dynamic vibrational analysis of a cracked and unbalanced Jeffcott rotor system with a disc at the middle and levitated by two foil bearings at the ends were presented in the article. Apart from this, a model-based identification algorithm relying on the full spectrum technique was also proposed to estimate simultaneously unbalance and crack faults, as well as foil bearings stiffness and damping coefficients.

Shaft displacement responses were generated at the disc location in the transverse directions and analyzed for distinct spin and ramp-up speed values. The shaft centreline orbit was found to have an eight-shaped curved trajectory and simultaneously asymmetric about axes, indicating cracks in the system at lower speeds. Moreover, the orbit plots were also observed to be circular at higher speeds due to the overpowering nature of unbalance force on the crack force. Further, to mimic the actual test response, different levels of Gaussian noise were added to the simulated response. It was observed that the shape of the displacement orbit was thicker at the high value of noise addition. The displacement at twice the spin speed was

maximum in the full spectrum plot. This was also an indicator of a crack fault in the rotor system. Various parameters such as eccentricity and phase values of unbalance fault, crack additive stiffness, as well as the stiffness and damping coefficients of foil bearings were excellently identified with a small amount of error even with the addition of noise signals and system modelling errors. This represents the effectiveness, accuracy, and robustness of the developed approach.

However, in the present paper, the considered rotor system was simple, in which the rotational degrees of freedom were neglected. The shaft stiffness, damping, gyroscopic effects, and non-linearity effects from foil-bearing supports were also not considered during mathematical modelling. Therefore, it is suggested to consider a foil-bearing levitated multi-disc flexible shaft system and model it using the finite element method in future work. Equations of motion of the flexible rotor system can be derived from Timoshenko beam theory. This will include the gyroscopic couple effect, shaft stiffness and damping effects, and nonlinearity from bearings. With the inclusion of these factors, the responses can be generated by solving the equations of motion, and further used in the identification algorithm to obtain higher accuracy in the estimation of system and fault parameters. Apart from this, the present article was based on only theoretical and numerical works. Hence, the experimental validation of the simulated rotor dynamic analysis and the proposed methodology would be an interesting scope of work in the future, by developing a laboratory test rig setup consisting of a rotor-foil bearing system.

References

[1] N. Bachschmid, P. Pennacchi, and A. Vania. Identification of multiple faults in rotor systems. *Journal of Sound and Vibration*, 254(2):327–366, 2002. doi: 10.1006/jsvi.2001.4116.

[2] J.W. Lund. Stability and damped critical speeds of a flexible rotor in fluid-film bearings. *Journal of Manufacturing Science and Engineering*, 96(2):509–517, 1974. doi: 10.1115/1.3438358.

[3] E.E. Swanson and H. Heshmat. Oil-free foil bearings as a reliable, high performance backup bearing for active magnetic bearings. In *ASME Turbo Expo 2002: Power for Land, Sea, and Air*, pages 589-598, Amsterdam, The Netherlands, 3-6 June 2002. doi: 10.1115/GT2002-30291.

[4] L. San Andrés and T.H. Kim. Gas foil bearings: limits for high-speed operation. In *World Tribology Congress III*, pages 71–72, Washington, D.C., USA, 12-16 September 2005. doi: 10.1115/WTC2005-63398.

[5] K. Feng and X. Zhao. Effects of misalignment on the structure characteristics of bump-type foil bearings: a comparison between experimental and theoretical results. *Industrial Lubrication and Tribology*, 67(4):370–379, 2015. doi: 10.1108/ILT-09-2013-0101.

[6] P. Kumar and R. Tiwari. Dynamic response analysis of an unbalanced and misaligned rotor supported on active magnetic bearings and touchdown bearings. In *Proceedings of the 6th National Symposium on Rotor Dynamics*, pages 407–418, NAL Bangalore, India, 2-3 July 2019. doi: 10.1007/978-981-15-5701-9_33.

[7] P. Kumar. Dynamic analysis and identification in a cracked and unbalanced rigid rotor with two offset discs and one middle disc mounted on foil bearings. *International Journal of Dynamics and Control*, 1–26, 2024. doi: 10.1007/s40435-024-01411-w.

[8] L. Rudloff, M. Arghir, O. Bonneau, and P. Matta. Experimental analyses of a first generation foil bearing: startup torque and dynamic coefficients. *Journal of Engineering for Gas Turbines and Power*, 133(9):092501, 2011. doi: 10.1115/1.4002909.

[9] C. Xiong, B. Xu, H. Yu, Z. Huang, and Z. Chen. Thermal failure optimization of foil thrust bearings. *International Journal of Mechanical Sciences*, 267:109026, 2024. doi: 10.1016/j.ijmecsci.2024.109026.

[10] J.-P. Peng and M. Carpino. Calculation of stiffness and damping coefficients for elastically supported gas foil bearings. *Journal of Tribology*, 115(1):20–27, 1993. doi: 10.1115/1.2920982.

[11] D. Rubio and L. San Andrés. Bump-type foil bearing structural stiffness: experiments and predictions. *Journal of Engineering for Gas Turbines and Power*, 128(3):653–660, 2006. doi: 10.1115/1.2056047.

[12] V. Arora, P.J.M. van der Hoogt, R.G.K.M. Aarts, and A. de Boer. Identification of stiffness and damping characteristics of axial air-foil bearings. *International Journal of Mechanics and Materials in Design*, 7:231–243, 2011. doi: 10.1007/s10999-011-9161-7.

[13] F. Balducchi, M. Arghir, and S. Gaudillere. Experimental analysis of the unbalance response of rigid rotors supported on aerodynamic foil bearings. In *Turbo Expo: Power for Land, Sea, and Air*, pages V07BT32A009, Düsseldorf, Germany, 16-20 June 2014. doi: 10.1115/GT2014-25552.

[14] J.S. Larsen, I.F. Santos, and S. von Osmanski. Stability of rigid rotors supported by air foil bearings: Comparison of two fundamental approaches. *Journal of Sound and Vibration*, 381:179–191, 2016. doi: 10.1016/j.jsv.2016.06.022.

[15] S.Y. Maraiy, W.A. Crosby, and H.A. El-Gamal. Thermohydrodynamic analysis of airfoil bearing based on bump foil structure. *Alexandria Engineering Journal*, 55(3):2473–2483, 2016. doi: 10.1016/j.aej.2016.06.015.

[16] Z. Guo, K. Feng, T. Liu, P. Lyu, and T. Zhang. Nonlinear dynamic analysis of rigid rotor supported by gas foil bearings: Effects of gas film and foil structure on subsynchronous vibrations. *Mechanical Systems and Signal Processing*, 107:549–566, 2018. doi: 10.1016/j.ymssp.2018.02.005.

[17] H. Li, P.H. Geng, and H. Lin. The performance of Generation II journal gas foil bearing with misalignment. *Industrial Lubrication and Tribology*, 72(7):857–863, 2020. doi: 10.1108/ILT-10-2019-0418.

[18] A. Martowicz, J. Roemer, S. Kantor, P. Zdziebko, G. Żywica, and P. Bagiński. Gas foil bearing technology enhanced with smart materials. *Applied Sciences*, 11(6):2757, 2021. doi: 10.3390/app11062757.

[19] J. Kumar, D.S. Khamari, S.K. Behera, and R.K. Sahoo. A methodology for performance prediction: aerodynamic analysis of axially loaded gas foil bearing. *Sādhanā*, 46:193, 2021. doi: 10.1007/s12046-021-01721-1.

[20] D.S. Khamari, J. Kumar, and S.K. Behera. A review on modeling and stability aspects of gas foil bearing supported rotors. *Tribology in Industry*, 45(1):12–23, 2023. doi: 10.24874/ti.1381.09.22.01.

[21] F. Xu, Z. Dong, H. Zhang, and Z. Xie. Vibration characteristics control of hybrid radial gas foil bearing-rotor system: Simulation and experiment. *Mechanical Systems and Signal Processing*, 198:110402, 2023. doi: 10.1016/j.ymssp.2023.110402.

[22] H. Guan, J. Li, K. Wei, and H. Zou. Rotordynamics of a rotor radially and axially supported by active bump-type foil bearings and bump-type thrust foil bearings. *Mechanical Systems and Signal Processing*, 208:110995, 2024. doi: 10.1016/j.ymssp.2023.110995.

[23] X. Zhao, C. Li, J. Du, and Y. Lu. A nonlinear model for dynamic performance analysis of gas foil bearing-rotor system considering frictional contacts. *Nonlinear Dynamics*, 112:5975–5996, 2024. doi: 10.1007/s11071-024-09309-0.

[24] O. Jun, H. Eun, Y. Earmme, and C.-W. Lee. Modelling and vibration analysis of a simple rotor with a breathing crack. *Journal of Sound and Vibration*, 155(2):273–290, 1992. doi: 10.1016/0022-460X(92)90511-U.

[25] R. Gasch. A survey of the dynamic behaviour of a simple rotating shaft with a transverse crack. *Journal of Sound and Vibration*, 160(2):313–332, 1993. doi: 10.1006/jsvi.1993.1026.

[26] C. Zhu, D.A. Robb, and D.J. Ewins. The dynamics of a cracked rotor with an active magnetic bearing. *Journal of Sound and Vibration*, 265(3):469–487, 2003. doi: 10.1016/S0022-460X(03)00174-3.

[27] A. Sekhar. Model-based identification of two cracks in a rotor system. *Mechanical Systems and Signal Processing*, 18(4):977–983, 2004. doi: 10.1016/S0888-3270(03)00041-4.

[28] P. Pennacchi, N. Bachschmid, and A. Vania. A model-based identification method of transverse cracks in rotating shafts suitable for industrial machines. *Mechanical Systems and Signal Processing*, 20(8):2112–2147, 2006. doi: 10.1016/j.ymssp.2005.04.005.

[29] S. Singh and R. Tiwari. Model based identification of crack and bearing dynamic parameters in flexible rotor systems supported with an auxiliary active magnetic bearing. *Mechanism and Machine Theory*, 122:292–307, 2018. doi: 10.1016/j.mechmachtheory.2018.01.006.

[30] H. Peng and Q. He. The effects of the crack location on the whirl motion of a breathing cracked rotor with rotational damping. *Mechanical Systems and Signal Processing*, 123: 626–647, 2019. doi: 10.1016/j.ymssp.2019.01.029.

[31] R. Gradzki, Z. Kulesza, and B. Bartoszewicz. Method of shaft crack detection based on squared gain of vibration amplitude. *Nonlinear Dynamics*, 98:671–690, 2019. doi: 10.1007/s11071-019-05221-0.

[32] A. Joshuva and V. Sugumaran. Crack detection and localization on wind turbine blade using machine learning algorithms: A data mining approach. *Structural Durability & Health Monitoring*, 13(2):181–203, 2019. doi: 10.32604/sdhm.2019.00287.

[33] Y. Yang, W. Xia, J. Han, Y. Song, J. Wang, and Y. Dai. Vibration analysis for tooth crack detection in a spur gear system with clearance nonlinearity. *International Journal of Mechanical Sciences*, 157: 648–661, 2019. doi: 10.1016/j.ijmecsci.2019.05.012.

[34] Y. Yongfeng, W. Qinyu, W. Yanlin, Q. Weiyang, and L. Kuan. Dynamic characteristics of cracked uncertain hollow-shaft. *Mechanical Systems and Signal Processing*, 124:36–48, 2019. doi: 10.1016/j.ymssp.2019.01.035.

[35] X. Zhang, Y. Yang, M. Shi, A. Ming, and P. Wang. Novel energy identification method for shallow cracked rotor system. *Mechanical Systems and Signal Processing*, 186:109886, 2023. doi: 10.1016/j.ymssp.2022.109886.

[36] Z. Qiao, K. Chen, C. Zhou, and H. Ma. An improved fault model of wind turbine gear drive under multi-stage cracks. *Simulation Modelling Practice and Theory*, 122:102679, 2023. doi: 10.1016/j.simpat.2022.102679.

[37] B. Han, Z. Liu, P. He, and P. Yan. Rotor crack breathing under unbalanced disturbance. *Journal of Sound and Vibration*, 574:118236, 2024. doi: 10.1016/j.jsv.2023.118236.

[38] P. Kumar, V. Kumar, K. Kumar, and L.S. Meena. Unbalance and dynamic parameters estimation in a rigid rotor mounted on active magnetic bearings. In *Advances in Applied Mechanical Engineering*, pages 363–371, NIT Warangal, India, 2-4 May 2019. doi: 10.1007/978-981-15-1201-8_41.

[39] A.K. Jardine, D. Lin, and D. Banjevic. A review on machinery diagnostics and prognostics implementing condition-based maintenance. *Mechanical Systems and Signal Processing*, 20(7):1483–1510, 2006. doi: 10.1016/j.ymssp.2005.09.012.

[40] J. Baker. Methods of rotor-unbalance determination. *Journal of Applied Mechanics*, 6(1):1–6, 1939. doi: 10.1115/1.4008884.

[41] K. Gupta, K. Gupta, and K. Athre. Unbalance response of a dual rotor system: theory and experiment. *Journal of Vibration and Acoustics*, 115(4):427–435, 1993. doi: 10.1115/1.2930368.

[42] Y.-P. Shih and A.-C. Lee. Identification of the unbalance distribution in flexible rotors. *International Journal of Mechanical Sciences*, 39(7):841–857, 1997. doi: 10.1016/S0020-7403(96)00078-1.

[43] S. Zhou and J. Shi. Active balancing and vibration control of rotating machinery: a survey. *Shock and Vibration Digest*, 33(5):361–371, 2001. doi: 10.1177/058310240103300501.

[44] M. De Queiroz. An active identification method of rotor unbalance parameters. *Journal of Vibration and Control*, 15:1365–1374, 2009. doi: 10.1155/2016/8284625.

[45] H.F. De Castro, K.L. Cavalca, L.W.F. De Camargo, and N. Bachschmid. Identification of unbalance forces by metaheuristic search algorithms. *Mechanical Systems and Signal Processing*, 24(6):1785–1798, 2010. doi: 10.1016/j.ymssp.2009.11.012.

[46] Y. Menshikov. Identification of rotor unbalance as inverse problem of measurement. *Advances in Pure Mathematics*, 3(9):20–25, 2013. doi: 10.4236/apm.2013.39A1004.

[47] P. Kumar and R. Tiwari. Finite element modelling, analysis and identification using novel trial misalignment approach in an unbalanced and misaligned flexible rotor system levitated by active magnetic bearings. *Mechanical Systems and Signal Processing*, 152:107454, 2021. doi: 10.1016/j.ymssp.2020.107454.

[48] Y. Zhang, Z. Xie, L. Zhai, and M. Shao. Unbalanced vibration suppression of a rotor with Rotating-Frequency faults using signal purification. *Mechanical Systems and Signal Processing*, 190:110153, 2023. doi: 10.1016/j.ymssp.2023.110153.

[49] S. Zhong and L. Hou. Numerical and experimental studies on unsupervised deep Lagrangian learning based rotor balancing method. *Science China Technological Sciences*, 66:1050-1061, 2023. doi: 10.1007/s11431-022-2102-3.

[50] K. Lin, Y. Li, Y. Wu, H. Fu, J. Jiang, and Y. Chen. A deep learning-based unbalanced force identification of the hypergravity centrifuge. *Sensors*, 23(8):3797, 2023. doi: 10.3390/s23083797.

[51] L.A. Baltazar-Tadeo, J. Colín-Ocampo, J.G. Mendoza-Larios, A. Abúndez-Pliego, M. Nango-Blanco, A. Blanco-Ortega, and S.J. Landa-Damas. An integrated balancing method for asymmetric rotor-bearing systems: algebraic identification, modal balancing, and active balancing disks. *Journal of Vibration Engineering & Technologies*, 11:619–645, 2023. doi: 10.1007/s42417-022-00598-6.

[52] Y. Kang, Z. Qiu, X. Huang, Z. Kong, F. Gu, and A.D. Ball. Field simultaneous estimation of residual unbalance and bearing dynamic coefficients for double-disk rotor-bearing system using dual augmented Kalman filter. *Journal of Sound and Vibration*, 577:118325, 2024. doi: 10.1016/j.jsv.2024.118325.

[53] R. Gasch. Dynamic behaviour of the Laval rotor with a transverse crack. *Mechanical Systems and Signal Processing*, 22(4):790–804, 2008. doi: 10.1016/j.ymssp.2007.11.023.

[54] S. Singh and R. Tiwari. Model-based fatigue crack identification in rotors integrated with active magnetic bearings. *Journal of Vibration and Control*, 23(6):980–1000, 2017. doi: 10.1177/1077546315587146.

[55] P. Kumar and R. Tiwari. Development of a novel approach for quantitative estimation of rotor unbalance and misalignment in a rotor system levitated by active magnetic bearings. *Iranian Journal of Science and Technology-Transactions of Mechanical Engineering*, 45:769–786, 2020. doi: 10.1007/s40997-020-00364-7.

[56] C. Shravankumar and R. Tiwari. Experimental identification of cracked rotor system parameters from the forward and backward whirl responses. *Archive of Mechanical Engineering*, 66(3):329–353, 2019. doi: 10.24425/ame.2019.129679.

[57] D.K. Roy and R. Tiwari. Development of identification procedure for the internal and external damping in a cracked rotor system undergoing forward and backward whirls. *Archive of Mechanical Engineering*, 66(2):133–152, 2019. doi: 10.24425/ame.2019.128446.

[58] N. Sarmah and R. Tiwari. Analysis and identification of the additive and multiplicative fault parameters in a cracked-bowed-unbalanced rotor system integrated with an auxiliary active magnetic bearing. *Mechanism and Machine Theory*, 146:103744, 2020. doi: 10.1016/j.mechmachtheory.2019.103744.

[59] L. Xiang, Y. Zhang, A. Hu, and F. Ye. Dynamic analysis and experiment investigation of a cracked dual-disc bearing-rotor system based on orbit morphological characteristics. *Applied Mathematical Modelling*, 80:17–32, 2020. doi: 10.1016/j.apm.2019.11.042.

[60] G. Ranjan and R. Tiwari. On-site high-speed balancing of flexible rotor-bearing system using virtual trial unbalances at slow run. *International Journal of Mechanical Sciences*, 183:105786, 2020. doi: 10.1016/j.ijmecsci.2020.105786.

[61] R. Tiwari and P. Kumar. An innovative virtual trial misalignment approach for identification of unbalance, sensor and active magnetic bearing misalignment along with its stiffness parameters in a magnetically levitated flexible rotor system. *Mechanical Systems and Signal Processing*, 167:108540, 2022. doi: 10.1016/j.ymssp.2021.108540.

[62] T.H. Patel and A.K. Darpe. Experimental investigations on vibration response of misaligned rotors. *Mechanical Systems and Signal Processing*, 23(7):2236–2252, 2009. doi: 10.1016/j.ymssp.2009.04.004.

[63] N. Sarmah and R. Tiwari. Dynamic analysis and identification of multiple fault parameters in a cracked rotor system equipped with active magnetic bearings: a physical model based approach. *Inverse Problems in Science and Engineering*, 28(8):1103–1134, 2019. doi: 10.1080/17415977.2019.1700982.

[64] P. Kumar and R. Tiwari. Dynamic analysis and identification of unbalance and misalignment in a rigid rotor with two offset discs levitated by active magnetic bearings: a novel trial misalignment approach. *Propulsion and Power Research*, 10(1):58–82, 2020. doi: 10.1016/j.jppr.2020.06.003.

[65] M. Lal. Modeling and estimation of speed dependent bearing and coupling misalignment faults in a turbine generator system. *Mechanical Systems and Signal Processing*, 151:107365, 2020. doi: 10.1016/j.ymssp.2020.107365.